Nonlinear magnetic dynamics in a nanomagnet–topological insulator heterostructure

Xiaopeng Duan, Xi-Lai Li, Yuriy G. Semenov, and Ki Wook Kim

Phys. Rev. B **92**, 115429 — Published 18 September 2015

DOI: 10.1103/PhysRevB.92.115429

Nonlinear magnetic dynamics in a nanomagnet–topological insulator heterostructure

Xiaopeng Duan,[1] Xi-Lai Li,[1] Yuriy G. Semenov,[1] and Ki Wook Kim[1,2,*]

[1]*Department of Electrical and Computer Engineering, North Carolina State University, Raleigh, NC 27695, USA*

[2]*Department of Physics, North Carolina State University, Raleigh, NC 27695, USA*

Abstract

Magnetization dynamics of a nanomagnet, when strongly coupled with a topological insulator (TI) via the proximity interaction, is examined theoretically in the presence of electrical current on the TI surface under realistic transport conditions. Due to the spin-momentum interlock, the magnetic state and TI electron transport depend significantly on each other. Such an interdependence leads to a variety of nonlinear dynamical responses in *all transport regimes* including the scattering dominant diffusive cases. Generation of the anomalous Hall current, in particular, is found to be a key to the unique features that have not been observed previously. For instance, the anomalous Hall current can result in antiparallel alignment of the final magnetization state in reference to the effective driving magnetic field by inducing an extra term that counters the damping effect. Similarly the calculation also reveals steady oscillation of the magnetization under a broad range of conditions, offering a robust mechanism for highly efficient magnetization reversal and/or spin wave excitation under a DC bias.

PACS numbers: 72.25.-b, 73.20.-r, 73.50.Jt, 85.75.-d

I. INTRODUCTION

Magnetic devices have been an essential component in the development of information technology. Information can be easily encoded into and decoded from the stable magnetization states of nanomagnets. Much effort has been devoted to improving the magnetization switching efficiency and reliability,[1–5] among which the search for electric control has been a major focus. For instance, the transition from the Ampere-field driven magnetic switches to the spin transfer torque (STT) driven counterparts has already seen significant advancements during the past decade. Apart from the applications to magnetic switches, the STT effect has also been shown to excite steady oscillations when the additional torque from spin transfer accurately cancels the magnetic damping effect.[1–3] In the case of magnetic insulators, where the STT mechanism is not applicable owing to the absence of free electrons, the electrical control can be achieved by exploiting the intrinsic multiferroic properties that exist in some crystal groups and heterostructures.[6–8] Most of them rely on the strain to mediate the piezoelectric and magnetostrictive effects. The magnetization orientations are restricted by the crystalline anisotropy that the strain can manipulate.

In the context of electric control of magnetization, the unique advantage of spin-momentum interlock in the topological insulators (TIs) offers a promising alternative.[9] The flow of electrons on a TI surface is naturally spin polarized; as such, an adjacent magnet in direct contact can potentially experience the exchange field through the proximity interaction and change its magnetization.[10–16] In this scenario, electron spin is the medium that couples the electrical variable (i.e., the electron momentum) with the magnetic variable (i.e., the magnetization of the adjacent magnet). Intuitively, the magnetization would align with the exchange field from the electron spin. However, electron transport on the TI surface is also strongly affected by the magnetization state,[17] thus forming a correlated nonlinear system. Complex dynamical behaviors can be expected.

Figure 1(a) illustrates a typical structure that utilizes the combination of a ferromagnetic insulator (FMI) and a TI. As indicated, the magnet (i.e., FMI) is in direct contact with the TI. Two surface electrodes are used to drive the electron flow through the interface region between the layers. An earlier theoretical investigation based on a self-consistent treatment of the TI-FMI system revealed the previously unidentified magnetic responses such as magnetization reversal and sustained oscillations under a DC bias condition.[12] The

key to this nontrivial outcome is the inter-dependent nature of the dynamics; namely, the spin polarized TI current modulating the magnetization via the effective magnetic field and conversely, the magnetization affecting the TI surface current via the electronic band modification. However, the study assumed coherent electron transport between the two contacts, greatly limiting the range of practical application at room temperature.

In a realistic device, the coherence is unlikely to hold even if electrons could travel through the magnetic barrier ballistically. Furthermore, a fully diffusive treatment may be more appropriate for a large device or with an imperfect sample, where substantial scattering is anticipated. Here, we extend the study of the coupled dynamic response to the practicable realm; i.e., the ballistic but non-coherent transport and the fully diffusive transport in the interface region of interest. The loss of coherence in both cases is attributed conveniently to the phase breaking events that electrons suffer in the TI surface channel before entering the portion covered by the FMI. This investigation aims at extending the coupled dynamics to all transport regimes and identifying the key influencing factors.

II. MODELS AND THEORETICAL ANALYSIS

The fully coupled dynamics must incorporate both the magnetization dependent TI surface transport and the influence of the surface current on the magnetization rotation. In the previously reported analysis,[12] the system was modeled essentially as the quantum mechanical wave tunneling through a barrier by coherently matching the boundary conditions at the two magnetic junctions. Thus the resultant solutions such as the magnetization state and the current exhibit the inherent dependence on the interference. Accordingly, it is rather difficult to discern if an observed nonlinear behavior is the consequence of the nontrivial magnetization dynamics or simply the interference effect. This is important since the latter phenomenon (i.e., interference), as mentioned above, is unlikely to survive at the ambient temperature. Moreover the model Hamiltonian that was based on a relatively simple form of the surface exchange interaction, may have missed out some of the more complex physical processes. For instance the impact of inter-band exchange−a source for the anomalous Hall effect−has not been considered.

The key difference in the non-coherent regime (i.e., the present study) is that each magnetic junction (or boundary) is treated independently and the electron transport between

them accounted for in a particle-like manner (no interference). The presence or absence of the scattering events while traveling in the TI region covered by the magnet just separates the diffusive vs. ballistic cases. When the electrons suffer no scattering (i.e., ballistic but non-coherent), the TI surface channel can be described by a classical double barrier problem. Then the total transmission may be given as $T_0/(2-T_0)$ [$= \sum_{i=0}^{\infty} T_0(1-T_0)^{2i}T_0$] by summing over all possible sequential transmission events.[18] Here, i represents the number of reflections back-and-forth between the two boundaries before the eventual passage and T_0 the probability associated with each boundary as discussed in the literature.[19] To be more specific, the transmission probability T_0 is obtained as a function of the magnetization $\mathbf{M}$, the electron energy E, and the lateral momentum k_y. Subsequently the channel conductance can be calculated by the usual Landauer formalism; viz., $G_{\mathbf{M}} \propto \sum_{k_y} \int T_{\mathbf{M}}(E, k_y) \frac{\partial f}{\partial E} dE$, where $T_{\mathbf{M}}(E, k_y) = T_0/(2 - T_0)$ and $f(E)$ is the Fermi-Dirac function. The corresponding current (J_x) is simply the linear product of the conductance $G_{\mathbf{M}}$ and the driving voltage V. The diffusive case, on the other hand, may be considered as two boundaries separated by an ohmic resistor in the middle. As such, three resistors connected in series could be an adequate description. The $\mathbf{M}$-dependent conductance at each junction can be obtained from T_0 following the Landauer approach (defined as $G^0_{\mathbf{M}}$ by setting $T_{\mathbf{M}} = T_0$ in the expression given above), while the additional resistance (R_c) of the diffusive channel is readily estimated from the electrical resistivity of the TI surface. Then, the current is simply given as V divided by the total resistance; i.e., $J_x = V/(R_c + \frac{2}{G^0_{\mathbf{M}}})$. Strictly speaking, the resistivity of the TI surface may also be affected by the band modification and thus potentially a function of $\mathbf{M}$. However, this effect appears relatively minor if the TI chemical potential is sufficiently away from the band extremum (see also the numerical values given in Sec. III). Accordingly, the standard models described above are expected to capture the key dependence of the driving current (J_x) on the magnetization. On the other hand, they do not account for the potential presence of the transverse current−the anomalous Hall effect. Indeed, this transverse current flow provides a key component as demonstrated later in the discussion. Again, the magnetization and the current are inter-dependent and must be solved for simultaneously.

Figures 1(b) and 1(c) illustrate schematically the mechanisms of the anomalous Hall current in the TI-magnet system. The in-plane magnetization along the $+x$ axis shifts the TI surface electronic dispersion and causes the transmitted electron to have a net momentum toward the $-y$ direction, resembling light transmission through the media with a refractive

index mismatch.[19] In the ballistic but non-coherent case (where the FMI length L is limited to the electron mean free path λ), the transmission through the two magnetic boundaries are independent processes as mentioned above and the trajectory beneath the magnet is determined by the refraction at the incoming edge [Fig. 1(b)]. Consequently, the net nonzero momentum along the $-y$ axis constitutes the anomalous Hall current that is accompanied by the corresponding $-x$ spin polarization via spin-momentum interlock. A detailed study of the quasi-optic behavior found the anomalous Hall current ratio β (i.e., the ratio between the anomalous Hall current and the driving current) to be around 0.5 that is also invariant to the direction of current flow.[19] As this Hall current concerns only the x component of the magnetization, it can be expresses as $J_y = -\beta_x m_x |J_x|$, where $\mathbf{m} = \mathbf{M}/|\mathbf{M}| = (m_x, m_y, m_x)$ denotes the FMI magnetization normalized to the saturation magnetization $|\mathbf{M}|$ ($\equiv M_0$). In the fully diffusive transport, on the other hand, it gives a negligible contribution as the refracted momentum would be quickly relaxed by scattering events (i.e., $\beta_x \approx 0$). Note that the current actually refers to the electron flux throughout the discussion; hence, there is a sign difference with the convention. Another point worth a comment is that the transverse electron flow is not induced when the driving current and the magnetization are aligned orthogonal to each other in the plane (e.g., m_x with the y-directional driving potential). Hence, the phenomenon discussed above deviates somewhat from the conventional anomalous Hall effect. Nevertheless it can cause a transverse current under a certain magnetization condition and is termed as such.

Unlike the in-plane component discussed above, the out-of-plane magnetization induces the transverse current under both ballistic and diffusive conditions [Fig. 1(c)].[20–23] A sizable anomalous Hall effect has been discovered in magnetically doped and magnet capped TIs, indicating the potential significance in the coupled magnetization-current response.[22–24] The physical origin of this phenomenon follows from the traditional models of the anomalous Hall effect, with the contributions of both the intrinsic and the extrinsic nature.[25] As it turns out, the intrinsic factors such as the field induced inter-band exchange have shown to be dominant in most TI materials.[20–23] Unfortunately, simple governing equations for the amplitude of the Hall current are yet to be provided in the literature due to the theoretical complexities. Nevertheless, there are sufficient results that lead to quasi-quantitative estimations with a degree of confidence. Similar to the in-plane counterpart, this component of the Hall current can be expressed as $J_y = -\beta_z m_z J_x$ with the corresponding ratio β_z. In comparison,

the earlier study based on the coherent treatment did not fully consider the Hall contribution by the z-magnetization for the lack of appropriate physical treatments.[12]

Following the description of the anomalous Hall effect given above, a qualitative picture of the coupled TI-magnet system can be developed. In the ballistic transport, both the in-plane ($\|\hat{\mathbf{x}}$) and the out-of-plane ($\|\hat{\mathbf{z}}$) magnetization can induce the anomalous Hall current ($\|\hat{\mathbf{y}}$), which brings additional spin polarization or the effective magnetic field that in turn affects the magnetization. On the other hand, just the effect of m_z needs to be considered in the diffusive transport because the m_x-induced anomalous Hall current exists only around the magnetic boundaries and, thus, becomes negligible in terms of the magnet as a whole. To circumvent the numerous unknowns in calculating the magnitude of the Hall effect, we treat the ratios $\beta_{x,z}$ as variables in the analysis around the values found in the literature (for instance, $\beta_z \approx 0.05$).[23,24,26] It is interesting to note that in most cases, the anomalous Hall current with $\beta_z > 0$ exhibited a p-type (hole-like) ordinary Hall character even though the examined TI samples could be both n-type and p-type.[24,26] The physical reason for this behavior is outside the scope of the present investigation. We assume that the TI sample is n-type and the anomalous Hall effect is larger than the ordinary Hall effect due to the magnet's stray field so that β_z is positive.

To compute the response of the coupled TI-FMI system, the expressions describing the TI surface current and those for the magnet must be solved simultaneously. With the driving current J_x and the corresponding anomalous Hall current $J_y = -\beta_x m_x |J_x| - \beta_z m_z J_x$, the net spin polarization can be expressed as $\mathbf{S} = \frac{J_y}{ev_F}\hat{\mathbf{x}} - \frac{J_x}{ev_F}\hat{\mathbf{y}}$ (v_F being the Fermi velocity). Considering the exchange magnetic field $\mathbf{H}_{ex} = (H_x, H_y, 0) = \frac{G}{\mu_0 L_z M_0}\mathbf{S}$, where L_z denotes the thickness of the magnet, μ_0 the permeability of vacuum, and G the TI-magnet exchange coupling energy, we have a well defined relation between the x and y components:

$$H_x = -\beta_x m_x |H_y| + \beta_z m_z H_y \,. \tag{1}$$

Then, the dynamics of the magnetic layer can be expressed in the Landau-Lifschitz (LL) equation as

$$\frac{\partial \mathbf{m}}{\partial t} = -\frac{\gamma}{1+\alpha^2}\mathbf{m} \times \mathbf{H}_{\text{tot}} - \frac{\gamma\alpha}{1+\alpha^2}\mathbf{m} \times (\mathbf{m} \times \mathbf{H}_{\text{tot}}) \,, \tag{2}$$

where γ is the gyromagnetic ratio and α the Gilbert damping factor. In addition, $\mathbf{H}_{\text{tot}}$ represents the total effective field that includes the TI-magnet exchange interaction (i.e.,

$\mathbf{H}_{ex}$) and the anisotropy field of the magnet. The inter-dependence between $\mathbf{J}$ and $\mathbf{m}$ makes it very difficult to get an analytical solution.

For a physical insight into the nontrivial influence of the anomalous Hall current, a simplified example is also considered before Eq. (2) is treated numerically. It can be readily recognized from Eq. (1) that the term containing β_x behaves essentially like an additional hard-axis anisotropy along the x axis with the anisotropy energy of $\frac{1}{2}\mu_0 M_0 \beta_x |H_y|$. The corresponding impact can be intuitively understood as lowering the barrier for the switching between the $\pm x$ magnetization. Once β_x and all of the anisotropy contributions are ignored (for the sake of the more interesting β_z), the total effective field is reduced to $\mathbf{H}_{\text{tot}} = (\beta_z m_z H_y \hat{\mathbf{x}} + H_y \hat{\mathbf{y}})$ and the right-hand side of Eq. (2) becomes

$$\begin{aligned} RHS &= \frac{\gamma}{1+\alpha^2} H_y \left[\begin{pmatrix} m_z \\ 0 \\ -m_x \end{pmatrix} + \beta_z m_z \begin{pmatrix} 0 \\ -m_z \\ m_y \end{pmatrix} \right] \\ &+ \frac{\gamma}{1+\alpha^2} H_y \left[\alpha \begin{pmatrix} -m_x m_y \\ 1-m_y^2 \\ -m_y m_z \end{pmatrix} + \alpha \beta_z m_z \begin{pmatrix} 1-m_x^2 \\ -m_x m_y \\ -m_x m_z \end{pmatrix} \right] \\ &= \frac{\gamma}{1+\alpha^2} H_y \begin{pmatrix} m_z - \alpha m_x m_y + \alpha \beta_z m_z \left(1-m_x^2\right) \\ (\alpha - \beta_z)\left(1-m_y^2\right) + \beta_z m_x^2 - \alpha \beta_z m_x m_y m_z \\ -m_x - (\alpha - \beta_z) m_y m_z - \alpha \beta_z m_x m_z^2 \end{pmatrix}. \end{aligned} \tag{3}$$

It is important to note that the terms containing α are associated with the damping while the rest drive the precession. In particular, the y-component of the above expression clearly illustrates the competition between the damping and the counter force that is induced by the anomalous Hall current [see the term with $(\alpha - \beta_z)$]. When β_z is set to zero (i.e., no Hall effect), the magnetization $\mathbf{m}$ would eventually settle along the direction parallel to H_y (i.e., the natural spin polarization of the driving current) after transient dynamics as in the conventional cases. If β_z becomes non-zero and larger than α, on the other hand, the resulting change of sign (i.e., $\alpha - \beta_z < 0$) could mean the final magnetization in the antiparallel orientation with H_y – a rather unprecedented prospect. In the limiting case of $\beta_z \approx \alpha$, a third possibility may be realized where the damping is effectively canceled and the magnetization enters into the state of sustained oscillations. The addition of the β_x term (in the ballistic transport) is not expected to qualitatively alter the picture since it essentially

mimics the hard-axis anisotropy.

III. NUMERICAL RESULTS AND DISCUSSION

For the detailed quantitative analysis, the magnetization dynamics of each transport condition is examined by numerically solving the LL equation in the presence of β_z, β_x, and magnetic anisotropy. Figure 2 shows the results for the diffusive transport as a function of the driving voltage V and the damping parameter α. In this case, β_x is set to zero due to its negligible contribution following the discussion given earlier. The magnet is assumed to have a dimension of $90 \times 40 \times 2.2$ nm^3 and the saturation magnetization of 1200 G. A hard-axis anisotropy of 2.5×10^4 J/m^3 along the y direction is also considered. In combination with other anisotropy terms, this in effect makes the x an overall easy axis for the magnet. We also suppose that Bi_2Se_3 is used as the TI layer with a chemical potential of $u_0 = 50$ meV (by setting the Dirac point as the reference) and the Fermi velocity $v_F = 4.6 \times 10^7$ cm/s. The resistivity of the TI surface is taken to be $\sim 10^3$ $\Omega/\square$ and the TI-magnet exchange constant $G = 40$ meV. For convenience, the bias is chosen such that electrons flow rightward and the resulting effective field points toward the $-y$ direction, i.e., $H_y < 0$. Consequently, the intuitive behavior for a normal magnet is to relax to the same (i.e., $-y$) direction. This is indeed the case as indicated in Fig. 2(a) when $\alpha = 0.08$. If the damping constant is smaller than the β_z factor, on the other hand, Fig. 2(b) with $\alpha = 0.01$ clearly illustrates that the final state could reverse and settle down to the opposite orientation ($m_y = 1$) in the manner consistent with the analysis based on Eq. (3). Note that both switching dynamics look almost identical except the final convergence points. The corresponding trajectories in the magnetization space are provided in Fig. 2(c) (see the blue vs. orange curves).

Another important consequence of the competition between α and β_z is the generation of steady oscillations when the two values are comparable, as illustrated in Fig. 2(d). While only 3 ns is plotted, the oscillations continue with negligible damping well past the simulated time of 10 ns. Furthermore, the resonant frequency is controllable via the applied voltage or the damping factor. Although α is often considered a fixed parameter for a given material, it can also be tuned through doping or by introducing nonmagnetic cap layers.[27,28] Along with the sustained oscillations, the random flip-flops between the $\pm x$ magnetization are possible as well before relaxing to a stable configuration [see Fig. 2(e)]. Figure 2(f) provides the

magnetization trajectories for both the oscillations and the flip-flops.

The multiplicity of the magnetization dynamics can be best represented by a "phase diagram" mapped on the V-α parameter space. In Fig. 3, the lines denote the boundaries between the different dynamical regimes while the background color indicates the characteristic frequency of magnetization rotation. Starting from the magnetization along the $+x$ direction, the responses can be identified as small deviations due to $\mathbf{H}_{ex}$, a flip (i.e., $-x$) or flip-flops between $\pm x$, alignment along H_y ($-y$), sustained or auto-oscillations, and antiparallel alignment to H_y ($+y$). Switching to $+y$ and the presence of auto-oscillations in a broad parameter space are the consequence of the anomalous Hall current (β_z). By contrast, other regimes (i.e., deviation and $-y$ alignment) can also be found in the ordinary dynamical processes. As each regime covers a well defined portion of the phase space, they are relatively robust against the fluctuations. The magnetization rotation frequencies are determined from the simulated magnetization dynamics. For the sustained oscillations, it is the generated (i.e., resonant) frequency. In the other regimes, the rotation period extracted near the final convergence point is used for simplicity. The frequency calculation also shows a tunable behavior with a gradual change except some abrupt transitions at the bifurcation boundaries. For instance, the frequency can be modulated by more than an order of magnitude in the range of approximately $1 \sim 10$ GHz for the sustained oscillations.

When the polarity of the bias reverses (i.e., with the electrons flowing leftward), the magnetization dynamics under the diffusive transport conditions remain virtually unaltered. Indeed, Fig. 4(a) is almost exactly an upside down version of Fig. 3;[29] note that the exchange field (H_y) induced by the spin-polarized surface current is now along the $+y$ direction. In comparison, the impact of the varying chemical potential is more substantial as it affects the results quantitatively even though the key dynamical characteristics are mostly alike [Fig. 4(b)]. The biggest deviation, however, is brought by the change in the Hall current factor β_z, particularly if it switches to a negative value. Figure 4(c) shows one such case where the damping is actually enhanced ($\alpha - \beta_z > \alpha$). Accordingly, the antiparallel alignment is no longer allowed while the auto-oscillation is limited to a very small region in the parameter space. Although it is not commonly seen, the possibility of a negative β_z is not excluded either with some preliminary indications of such from recent experimental results.[24,26]

As electron transport in the interface region becomes collision-free (i.e., $L \lesssim \lambda$), the in-

fluence of β_x must be accounted for in combination with the momentum refraction at the boundaries. Figure 5(a) shows the calculation result with $\beta_x = 0.6$. When compared to the corresponding case in the diffusive transport (Fig. 3), the key features are rather alike except that the required biases are substantially smaller. The reduction in the voltage may be attributed to the equivalent hard-axis anisotropy provided by β_x as well as the negligible (or zero) ohmic potential. The similarities between the two figures indicate the relative insignificance of β_x in comparison to β_z. This is further verified in Fig. 5(b) when β_z is artificially set to zero. Consistent with the earlier discussion, a substantially different picture emerges with the disappearance of the antiparallel alignment regime and the narrowed parameter space for the oscillations (to small α). The case with both $\beta_{x,z} = 0$ is also shown in Fig. 5(c) for reference. With the exception of antiparallel alignment, it is remarkable to see the other responses maintained under such a drastic change in the Hall coefficients $\beta_{x,z}$. The calculation clearly indicates the nonlinearly coupled nature of the dynamics between the TI electrons and the magnetization of the magnet even in the absence of the anomalous Hall effect.

It is worth noting that our results may serve as a theoretical guidance for experimental verification. The parametric investigation illustrates the critical transitions between the different phases of dynamics. While the magnetic insulators often have a small damping factor (< 0.01), there are other factors that could further facilitate the multiplicity of dynamical behaviors. For one, the coefficients for the anomalous Hall effect are certainly sample dependent and can be substantially smaller than those used in the present study. This tends to shift the transition points (or lines) in the phase diagram toward the lower values of α [see, for example, Fig. 5(a) vs. Figs. 5(b,c)], exposing broader operation spectra. Additional measurement data are necessary for a more accurate analysis. Finally, the models and phenomena discussed here apply only to the insulating magnets. The interaction between TI electrons and the magnetic insulator is most suitably treated with the exchange field. For a metallic magnet, on the other hand, there could be spin polarized electrons injected to the metal as well as a shunt current through it. Thus, the spin transfer torque model would be more appropriate.[30] Plus, the electron transport on the TI surface also needs reconsideration as the metal may pin the Fermi level.

IV. SUMMARY

The strongly coupled dynamics of electron transport and magnetization switching is theoretically investigated in the TI-magnet hybrid structure in the realistic transport regimes. The nontrivial dynamics predicted earlier in a quantum mechanical wave-like analysis are similarly observed in the particle-like treatment, indicating the physically robust nature of these phenomena beyond the simple interference effect in the calculation. Further, the results illustrate an additional, unusual possibility of antiparallel alignment between the magnet magnetization and the driving exchange field when the anomalous Hall effect dominates over the normal damping process. The investigation also reveals that some of these nonlinear magnetization responses (such as the flip-flop and auto-oscillation) are rather prevalent and can be achieved under a broad range of anomalous Hall conditions as well as the transport regimes including the diffusive cases. Accordingly, the proposed mechanism of magnetization control is expected to offer a highly efficient alternative to the STT or spin-Hall based approaches. In particularly, the auto-oscillation phenomenon can provide a compact and low-power solution for spin wave generation with a range of practical applications.[31–37]

Acknowledgments

This work was supported, in part, US Army Research Office and FAME (one of six centers of STARnet, a SRC program sponsored by MARCO and DARPA).

* Electronic address: kwk@ncsu.edu

[1] J.-G. Zhu and C. Park, Materials Today **9**, 36 (2006).

[2] K. L. Wang, J. G. Alzate, and P. K. Amiri, J. Phys. D: Appl. Phys. **46**, 074003 (2013).

[3] S. Ikeda, J. Hayakawa, Y. M. Lee, F. Matsukura, Y. Ohno, T. Hanyu, and H. Ohno, IEEE Trans. Electron Devices **54**, 991 (2007).

[4] S. Kanai, M. Yamanouchi, S. Ikeda, Y. Nakatani, F. Matsukura, and H. Ohno, Appl. Phys. Lett. **101**, 122403 (2012).

[5] J.-M. Hu, Z. Li, L.-Q. Chen, and C.-W. Nan, Nat. Commun. **2**, 553 (2011).

[6] W. Eerenstein, N. D. Mathur, and J. F. Scott, Nature **442**, 759 (2006).

[7] H. Yu, O. d'Allivy Kelly, V. Cros, R. Bernard, P. Bortolotti, A. Anane, F. Brandl, R. Huber, I. Stasinopoulos, and D. Grundler, Sci. Rep. **4** (2014).

[8] C. A. F. Vaz, J. Phys.: Condens. Matter **24**, 333201 (2012).

[9] M. Z. Hasan and C. L. Kane, Rev. Mod. Phys. **82**, 3045 (2010).

[10] Y. G. Semenov, X. Duan, and K. W. Kim, Phys. Rev. B **86**, 161406 (2012).

[11] T. Yokoyama, Phys. Rev. B **84**, 113407 (2011).

[12] Y. G. Semenov, X. Duan, and K. W. Kim, Phys. Rev. B **89**, 201405 (2014).

[13] I. Garate and M. Franz, Phys. Rev. Lett. **104**, 146802 (2010).

[14] T. Yokoyama, Y. Tanaka, and N. Nagaosa, Phys. Rev. B **81**, 121401 (2010).

[15] T. Yokoyama, J. Zang, and N. Nagaosa, Phys. Rev. B **81**, 241410 (2010).

[16] A. Sakai and H. Kohno, Phys. Rev. B **89**, 165307 (2014).

[17] B. D. Kong, Y. G. Semenov, C. M. Krowne, and K. W. Kim, Appl. Phys. Lett. **98**, 243112 (2011).

[18] S. Datta, *Electronic Transport in Mesoscopic Systems* (Cambridge University Press, Cambridge, 1995).

[19] X. Duan, X. Li, Y. G. Semenov, and K. W. Kim, J. Appl. Phys. **116**, 224301 (2014).

[20] D. Culcer, Physica E **44**, 860 (2012).

[21] D. Culcer and S. Das Sarma, Phys. Rev. B. **83**, 245441 (2011).

[22] J. G. Checkelsky, R. Yoshimi, A. Tsukazaki, K. S. Takahashi, Y. Kozuka, J. Falson, M. Kawasaki, and Y. Tokura, Nat. Phys. **10**, 731 (2014).

[23] L. D. Alegria, H. Ji, N. Yao, J. J. Clarke, R. J. Cava, and J. R. Petta, Appl. Phys. Lett. **105**, 053512 (2014).

[24] C.-Z. Chang, J. Zhang, M. Liu, Z. Zhang, X. Feng, K. Li, L.-L. Wang, X. Chen, X. Dai, Z. Fang, X.-L. Qi, S.-C. Zhang, Y. Wang, K. He, X.-C. Ma, and Q.-K. Xue, Adv. Mater. **25**, 1065 (2013).

[25] N. Nagaosa, J. Sinova, S. Onoda, A. H. MacDonald, and N. P. Ong, Rev. Mod. Phys. **82**, 1539 (2010).

[26] J. Zhang, C.-Z. Chang, P. Tang, Z. Zhang, X. Feng, K. Li, L. Wang, X. Chen, C. Liu, W. Duan, K. He, Q.-K. Xue, X. Ma, and Y. Wang, Science **339**, 1582 (2013).

[27] C. Luo, Z. Feng, Y. Fu, W. Zhang, P. K. J. Wong, Z. X. Kou, Y. Zhai, H. F. Ding, M. Farle, J. Du, and H. R. Zhai, Phys. Rev. B **89**, 184412 (2014).

[28] Y. Sun, H. Chang, M. Kabatek, Y.-Y. Song, Z. Wang, M. Jantz, W. Schneider, M. Wu, E. Montoya, B. Kardasz, B. Heinrich, S. G. E. te Velthuis, H. Schultheiss, and A. Hoffmann, Phys. Rev. Lett. **111**, 106601 (2013).

[29] This symmetry with respect to the bias polarity illustrates a clear departure from the coherent dynamics, where the invariant is over the simultaneous reversal of both the magnetization and the driving bias as described in Ref. 12.

[30] A. R. Mellnik, J. S. Lee, A. Richardella, J. L. Grab, P. J. Mintun, M. H. Fischer, A. Vaezi, A. Manchon, E.-A. Kim, N. Samarth, and D. C. Ralph, Nature **511**, 449 (2014).

[31] T. Schneider, A. A. Serga, B. Leven, B. Hillebrands, R. L. Stamps, and M. P. Kostylev, Appl. Phys. Lett. **92**, 022505 (2008).

[32] K.-S. Lee and S.-K. Kim, J. Appl. Phys. **104**, 053909 (2008).

[33] A. Khitun, D. E. Nikonov, and K. L. Wang, J. Appl. Phys. **106**, 123909 (2009).

[34] M. P. Kostylev, A. A. Serga, T. Schneider, B. Leven, and B. Hillebrands, Appl. Phys. Lett. **87**, 153501 (2005).

[35] A. Khitun, M. Bao, and K. L. Wang, IEEE Trans. Magn. **44**, 2141 (2008).

[36] K. Sekiguchi, K. Yamada, S. M. Seo, K. J. Lee, D. Chiba, K. Kobayashi, and T. Ono, Appl. Phys. Lett. **97**, 022508 (2010).

[37] Y. Kajiwara, K. Harii, S. Takahashi, J. Ohe, K. Uchida, M. Mizuguchi, H. Umezawa, H. Kawai, K. Ando, K. Takanashi, S. Maekawa, and E. Saitoh, Nature **464**, 262 (2010).

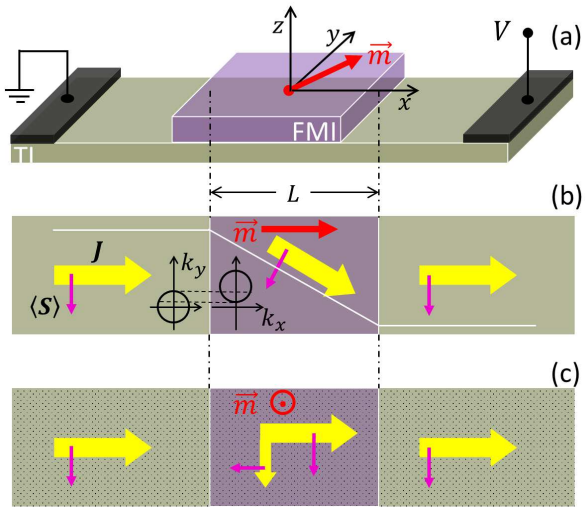

FIG. 1: (Color online) (a) Schematic illustration of the TI-magnet structure under investigation. An insulating nanomagnet (FMI) is placed on top of a TI surface, where two electrodes are used to inject the current through the TI-FMI interface region. The red arrow ($\vec{m}$) denotes the magnetization of the magnet. (b) and (c) show the mechanisms for the transverse current (i.e., the anomalous Hall effect) due to the in-plane and the out-of-plane magnetization, respectively. The thick arrows (yellow) represents the electron flow while the thin arrows (red) denote the corresponding spin polarization. The inset in (b) illustrates the shift of the iso-energy contour in the momentum space (TI) due to the in-plane magnetization (FMI).

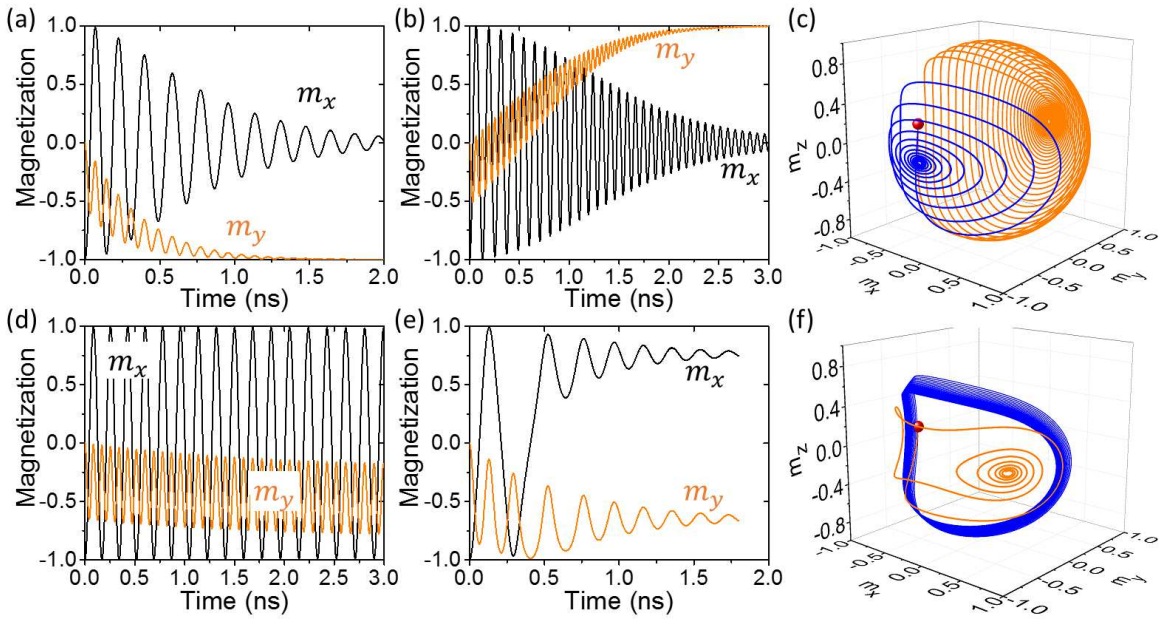

FIG. 2: (Color online) Dynamical response of the magnetization from the initial state $m_x = -1$ calculated under diffusive transport conditions (i.e., $\beta_x = 0$) with $\beta_z = 0.06$ at different driving voltages V and damping constants α: (a) $V = 0.25$ V, $\alpha = 0.08$; (b) $V = 0.25$ V, $\alpha = 0.01$; (d) $V = 0.2$ V, $\alpha = 0.03$; (e) $V = 0.15$ V, $\alpha = 0.07$. (c) and (f) show the corresponding trajectories in the magnetization space. The blue (dark) and orange (light) curves in (c) represent the results of (a) and (b), respectively. Similarly in (f), they are for (e) (blue) and (d) (orange). The red dot marks the initial state. The length L of 90 nm and the TI chemical potential u_0 of 50 meV are assumed in all cases.

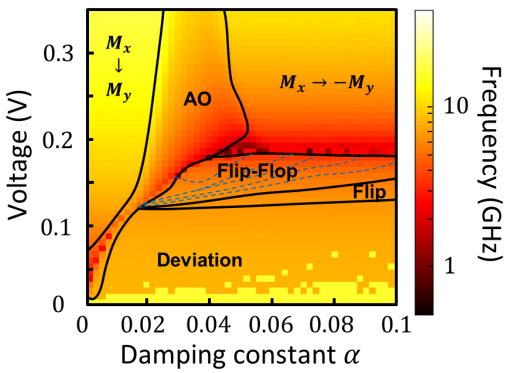

FIG. 3: (Color online) Magnetization dynamics mapped on the V-α parameter space. As in Fig. 2, the diffusive electron transport is considered with β_z fixed at 0.06. The solid lines separate the different dynamical regimes. The dashed lines in the flip-flop region indicate the smeared nature of the boundaries between the two final states ($+x$ or $-x$) after the precession. The background color provides the corresponding frequency of the magnetization rotation. AO stands for auto (or sustained) oscillations.

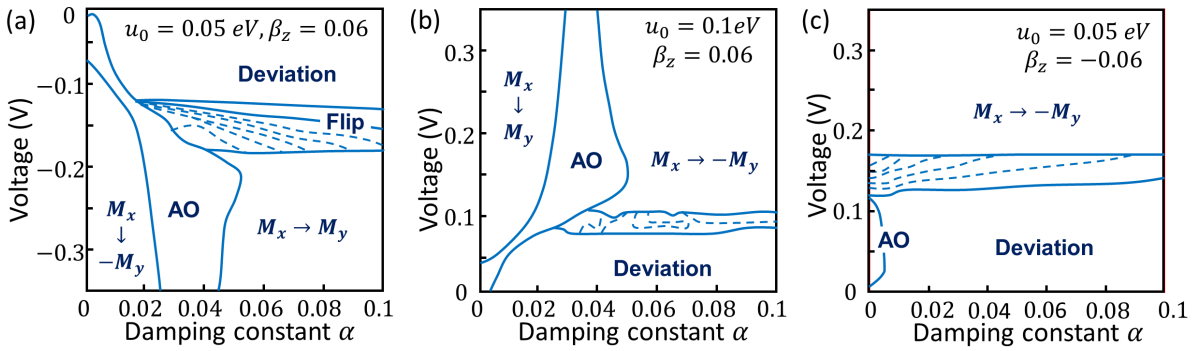

FIG. 4: (Color online) Phase diagram of the magnetization dynamics with (a) a reversed bias ($V < 0$), (b) a different TI chemical potential u_0, and (c) a negative β_z. The rest of the conditions and the notations are the same as in Fig. 3.

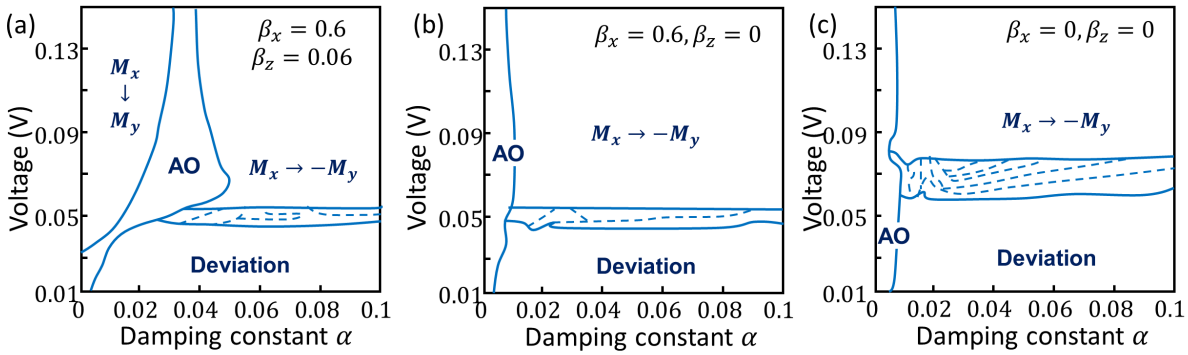

FIG. 5: (a) Magnetization dynamics calculated under ballistic but non-coherent transport conditions with $\beta_z = 0.06$ and $\beta_x = 0.6$. (b) and (c) examine hypothetical cases with the specified conditions for reference. The rest of the parameters and the notations remain the same as in Fig. 3.